frontiers | Frontiers in Marine Science

TYPE Original Research
PUBLISHED 04 September 2024
DOI 10.3389/fmars.2024.1410183



OPEN ACCESS

EDITED BY
Renato S. Carreira,
Pontifical Catholic University of Rio de Janeiro, Brazil

REVIEWED BY
Solomon Dan,
Beibu Gulf University, China
Alberto Sánchez-González,
National Polytechnic Institute (IPN), Mexico

*CORRESPONDENCE
Pei Sun Loh
psloh@zju.edu.cn

RECEIVED 31 March 2024
ACCEPTED 16 August 2024
PUBLISHED 04 September 2024

CITATION
Guo C, Loh PS, Hu J, Chen Z, Pradit S, Oeurng C, Sok T, Mohamed CAR, Lee CW, Bong CW, Lu X, Anshari GZ, Kandasamy S and Wang J (2024) Factors influencing mangrove carbon storage and its response to environmental stress.
*Front. Mar. Sci.* 11:1410183.
doi: 10.3389/fmars.2024.1410183



# Factors influencing mangrove carbon storage and its response to environmental stress

Chuanyi Guo[1], Pei Sun Loh[1]*, Jianxiong Hu[1], Zengxuan Chen[1], Siriporn Pradit[2], Chantha Oeurng[3], Ty Sok[3], Che Abd Rahim Mohamed[4], Choon Weng Lee[5,6], Chui Wei Bong[5,6], Xixi Lu[7], Gusti Z. Anshari[8], Selvaraj Kandasamy[9] and Jianjun Wang[10,11]

[1]Institute of Marine Geology and Resources, Ocean College, Zhejiang University, Zhoushan, China, [2]Coastal Oceanography and Climate Change Research Center, Faculty of Environmental Management, Prince of Songkla University, Hat Yai, Thailand, [3]Faculty of Hydrology and Water Resources Engineering, Institute of Technology of Cambodia, Phnom Penh, Cambodia, [4]Faculty of Science and Technology, Universiti Kebangsaan Malaysia, Bangi, Malaysia, [5]Institute of Ocean and Earth Sciences, Universiti Malaya, Kuala Lumpur, Malaysia, [6]Faculty of Science, Universiti Malaya, Kuala Lumpur, Malaysia, [7]Department of Geography, National University of Singapore, Singapore, Singapore, [8]Soil Science Department, Faculty of Agriculture, Tanjungpura University, Pontianak, Indonesia, [9]Department of Geology, School of Earth Sciences, Central University of Tamil Nadu, Thiruvarur, India, [10]Jiangsu Key Laboratory of Crop Genetics and Physiology/Jiangsu Key Laboratory of Crop Cultivation and Physiology, Agricultural College of Yangzhou University, Yangzhou, China, [11]Jiangsu Co-Innovation Centre for Modern Production Technology of Grain Crops, Yangzhou University, Yangzhou, China

Mangrove forests serve as significant carbon sinks and play a crucial role in mitigating climate change. Currently, the response of mangroves to intensified climate change and human activities, and the factors that influence the magnitude of carbon storage in their sediments remain uncertain. To address these questions, two sediment cores were collected from the mangrove reserve in Pearl Bay, Guangxi, China. The activity of $^{210}$Pb in the sediment, grain size, bulk elemental composition, stable carbon isotopes, lignin, and different sediment organic matter (OM) fractions were investigated to determine the local mangrove's response to climate change and human activities, as well as the factors influencing its carbon storage. The results showed mangrove forests with lower tidal ranges, slower sedimentation rates, and where OM predominantly originated locally tend to have larger carbon stocks. The mangrove OM (MOM) decreased progressively from the bottom to the top of the cores, indicating that the mangroves in Pearl Bay have possibly undergone degradation, which was further substantiated by the decrease in lignin content. Based on these results, the entire cores were divided into two stages: stable stage 1 (1963–2001) and degradation stage 2 (2001–2020). The cause of the mangrove degradation is likely due to the impact of human activities; however, these impacts are anticipated to gradually lessen in the future due to mangrove protection policies. Our results indicate that lignin can track and predict mangrove growth trends and provide guidance for the sustainable management of mangrove ecosystems.

KEYWORDS

**blue carbon ecosystem, sediment carbon storage, lignin biomarker, sea level rise, human disturbance**

# 1 Introduction

Mangrove forests are wetland plant communities comprising of salt-tolerant woody halophytes growing in the inter tidal zone of tropical and subtropical coasts. These forests play an important role in dissipating winds and waves, purifying seawater, maintaining biodiversity, and so on (Gao et al., 2019; Medina-Contreras et al., 2024). Mangrove ecosystems have high primary productivity of approximately 92–280 Tg carbon per year, and the carbon stored in mangrove soil is much higher than that in other macrophyte ecosystems (Bouillon et al., 2008; Alongi, 2014). Although mangrove forests make up only 0.1% of Earth's land area, their excellent ecosystem service and carbon storage capacity can help humanity cope with the threats posed by climate change (Atwood et al., 2017; Cavanaugh et al., 2019).

The global mangrove forest area decreased by 520,000 ha between 1996 and 2020, with an estimated loss of 3.4% over 24 years (Bunting et al., 2022), due to the effects of both climate change and human activities. Global warming has caused mangroves encroachment into salt marshes (Doughty et al., 2015), while erosion, land subsidence, and soil degradation cause a reduction in mangrove area (Giri and Long, 2014). The rise in sea level caused by climate change compresses the living spaces of mangrove forests and forces mangrove ecosystems to migrate toward the land (Alongi, 2015). Changes in temperature and rainfall affect phenological patterns, such as seed germination and flowering time, and species composition (Ward et al., 2016). Water vapor deficit and high salt conditions caused by excessive temperature affect the growth and development of mangrove forests, eventually leading to their degradation (Adame et al., 2021; Alongi, 2021). Mangrove forests face a greater threat from human activities than climate change, as 62% of global mangrove loss from 2000 to 2016 was attributed to human activities; this loss is primarily due to the conversion of mangrove forests for aquaculture and agriculture purposes (Goldberg et al., 2020). These natural and anthropogenic factors can cause additional fluctuations in mangrove area over shorter time scales, potentially altering mangrove carbon stocks (Comeaux et al., 2012).

The majority of sediment organic carbon (SOC) in mangrove sediments is stored in the top 1 meter of sediment, playing a crucial role in regulating carbon cycle and ecosystem functions (Kauffman et al., 2020). Due to the complexity of mangrove growth environments, the carbon stocks in mangrove sediments may be influenced by multiple factors, for instance, physio-chemical factors of the soil such as pH and salinity (Gao et al., 2019), types of mangrove vegetation (Wang et al., 2013), and climate factors (Kauffman et al., 2011). Xin et al. (2018) found that the carbon stock in the *Sonneratia caseolaris* community of Dongzhai Port mangroves was greater than that in the *Bruguiera sexangula* community due to greater biomass and growth density of *Sonneratia caseolaris*. The sources of organic carbon (OC) input into sediments can also affect the carbon stocks, as different OC sources have different carbon sequestration mechanisms (Sun et al., 2019). Additionally, the output of OC significantly determines the size of the carbon stock in the sediments. Collins et al. (2017) found that higher tidal range and stronger tidal currents promote mangrove organic matter (MOM) input, and Perez et al. (2018) suggested that different hydrological and tidal conditions can affect the deposition rate and carbon stock in mangrove forests. Currently, the impact of tidal range on mangrove carbon stocks remains unclear, and there are few related reports.

When mangrove forests undergo degradation or destruction, the physicochemical properties of the sediment may undergo changes, making stored carbon more vulnerable to mobilization, loss, and conversion to carbon dioxide, which is then released into the atmosphere (Friesen et al., 2018; Arias-Ortiz et al., 2020). Therefore, it is necessary to use biogeochemical indicators in sediment archives to reconstruct the historical dynamics of mangroves in order to assess changes in mangrove carbon stocks (Ellison, 2008). The evolutionary history of mangroves can be reconstructed through the sources of OC determined by the stable isotope characteristics ($\delta^{13}C$) and the ratio of total OC (TOC) to total nitrogen (TN) (C/N) in sediments (Lamb et al., 2006; Xiong et al., 2018a; Sánchez and Gómez-León, 2024). However, the redistribution of mangrove litter by surface runoff and tides, along with the overlapping $\delta^{13}C$ and C/N values of allochthonous source OM, poses a challenge in accurately reconstructing the evolutionary history of mangroves using this method (Cloern et al., 2002; Lamb et al., 2006). Therefore, the crucial aspect lies in ensuring that the $\delta^{13}C$ and C/N values precisely reflect the contribution of MOM. Mangrove pollen in sediments is a direct and effective proxy, widely used to validate the accuracy of MOM indicated by $\delta^{13}C$ and C/N values and to trace the historical development of Holocene mangroves (Li et al., 2008). Xia et al. (2015) employed chemical tracers ($\delta^{13}C$ and C/N) and isotope mixing models to quantify the contribution of MOM while compensating for the influence of diagenetic changes on stable isotope values by introducing mangrove pollen relative abundance. Meng et al. (2016) used a similar method to reconstruct the growth period, gradual degradation period, and rapid degradation period of the Maowei Sea mangroves in southwestern China over the past 130 years. However, the applicability of this method relies on the availability of adequate pollen content within the sediment, and the acquisition of reliable and accurate pollen data incurs a significant cost (Versteegh et al., 2004). Lignin, due to its source specificity and high resistance to degradation, is considered an effective indicator for tracing terrestrial organic matter (OM), similar to the ratios of $\delta^{13}C$ and C/N (Jex et al., 2014). Prasad and Ramanathan (2009) used the ratio of lignin phenols in sediments to determine that mangrove leaves were the primary source of terrestrial OM in the Pichavaram estuarine mangroves in India. Vaughn et al. (2020) found that the invasion of mangroves into salt marshes led to an increase in woody tissue input to the soil, which further promotes the increase in soil carbon stocks. However, there are few studies that utilize lignin to help reconstruct the development history of mangroves. Exploring the feasibility of using lignin biomarkers to reconstruct the evolutionary history of mangroves is crucial for a comprehensive understanding of their

responses to future climate change (Gilman et al., 2007). This study aims to achieve three objectives: 1) Compare mangroves in other regions to explore the effects of tidal range, sedimentation rate, and sources of OC on mangrove carbon stocks., 2) Use lignin biomarkers to infer the evolutionary development history of mangroves., and 3) Investigate the response of mangrove carbon stocks to external environmental pressures.

# 2 Materials and methods

## 2.1 Study area

Guangxi has a typical subtropical marine monsoon climate. In this area, the mean annual air temperature is 22.5°C, the coldest month is January, with an average temperature of 14.3°C (Li et al., 2015), the annual precipitation is 1,658 mm, and the mean sunshine duration is 1,673 h (Tian et al., 2021). Guangxi has approximately 8,715 ha of mangrove forests, and the main mangrove species are *Sonneratia apetala*, *Aegiceras corniculatum*, *Kandelia obovata*, *Avicennia marina*, *Rhizophora stylosa*, and *Bruguiera gymnorrhiza* (Zheng and Takeuchi, 2020). Pearl Bay is a semi-enclosed sea bay located in the city of Fangcheng Harbor, Guangxi, China. Pearl Bay covers an area of 94 $km^2$ and has a mouth length of 3.5 km. Two freshwater-dominated rivers flow into Pearl Bay: the Huangzhu and Xinlu Rivers (Fan et al., 2017). The diurnal average tide height in Pearl Bay is 2.24 m, the highest tide is 5.00 m (Chen et al., 2021), with an average salinity of 23.1‰ (Xu et al., 2020). The study area was a creek discharging into Pearl Bay (Figure 1A).

The natural mangrove forest in the sampling site is distributed in the intertidal zone, with an average tree age of 50 years. *Halophila beccarii* (Seagrass bed) are found on tidal flats at the edge of the mangrove forest. Some pioneering *Avicennia* trees grow in the mudflats in the low tide area. Mangrove species in the sampling site were *A. corniculatum*, *B. gymnorrhiza*, *A. marina*, and *K. obovata*. Underground aquaculture systems were built near the study area by burying plastic pipes in mud (Chen et al., 2021).

## 2.2 Sample collection and pretreatment

Two sediment cores were collected from a creek in a natural mangrove forest on the northeast side of Pearl Bay (Figure 1A) at GX1 (108°14′28″E, 21°37′2″N) and GX2 (108°14′21″E, 21°37′3″N) (Figure 1B) on June 30, 2021 using a gouge auger sampler (diameter: 6 cm; length: 100 cm) with minimal compaction. The sediment cores GX1 and GX2 were 88 and 96 cm long, respectively. At the sampling sites, the layers of sediment cores were sliced at every 2 cm, and the sub-samples were stored in polyethylene bags at low temperature (4°C). Drying of sediment samples at 45°C for two days (until constant weight) was completed within one week after sampling. The difference in mass of the sediment before and after drying in a 105°C oven was divided by the dry weight of the sediment to obtain the sediment moisture content, expressed as percentage dry weight.

## 2.3 Grain size analyses

Each sub-sample was treated with 20 ml $H_2O_2$ (40%) for 24 h to remove OM, followed by thorough rinsing with deionized water. Then, 10 ml of 1 M HCl was added to the residue to remove

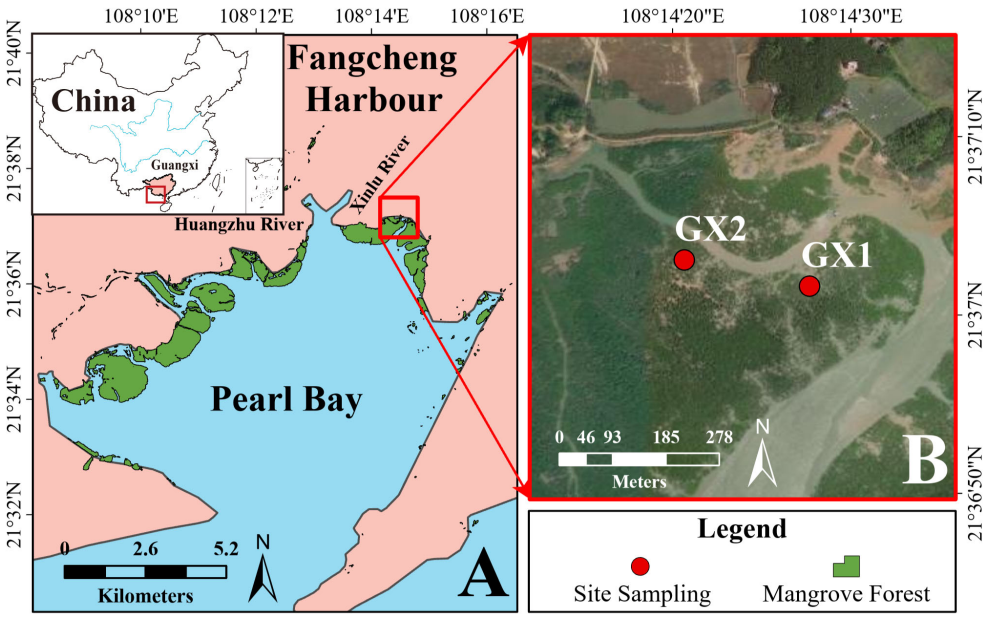


FIGURE 1
Map showing **(A)** the locations of Fangcheng Harbor (pink), Pearl Bay (blue), and mangrove forests (green) surrounding Pearl Bay, southern China; and **(B)** a high-resolution satellite image of the sampling sites (GX1 and GX2) in the natural mangrove forest.

inorganic matter, this was allowed to react for 2 h until no more bubbles were produced. After the reaction was complete, the samples were rinsed with deionized water until the pH of the wash water was neutral. Tetrasodium pyrophosphate (2%) was used to disperse the sub-samples, and grain size was then determined using the particle size analyzer Mastersizer 2,000 (Malvern, England), which measures particle size ranging from 0.02 μm to 2,000 μm. Grain size was divided into three categories, namely, clay (< 4 μm), silt (4–63 μm), and sand (63–2000 μm). The lithology of the sub-sample was determined using the Shepard triangle method (Shepard, 1954). The mean grain size, standard deviation, skewness, and kurtosis of the sub-samples were calculated using the calculation procedure created by Blott and Pye (2001).

## 2.4 Bulk elemental and stable carbon isotope analyses

The freeze-dried sub-samples were treated with HCl (1 M) to eliminate inorganic carbon until no bubbles were produced. The sediments were then dried in an oven, homogenized, and analyzed for TN and TOC using an elemental analyzer (EA3000, EuroVector, Italy). The molar ratio of TOC and TN was calculated and henceforth known as C/N ratio.

Stable carbon isotope ratios were analyzed using a stable isotope mass spectrometer (Delta V + EA Isolink, Thermo Fisher Scientific, USA). The C/N ratios and $\delta^{13}C$ of sediments in mangrove ecosystems have been extensively used to identify the sources of OM in mangrove sediments (Xiong et al., 2018b; Sasmito et al., 2020). OM from terrestrial $C_3$ plants, such as mangroves, with abundant cellulose exhibit a high C/N ratio (> 12) and low $\delta^{13}C$ values (< -21‰), whereas OM from marine end-members, such as phytoplankton, with abundant protein have lower C/N ratio (5–7) and higher $\delta^{13}C$ values (> -23‰) (Meyers, 1994; Lamb et al., 2006).

## 2.5 Radioisotope ($^{210}Pb$) analysis

Approximately 5 g of the freeze-dried sub-samples were weighed and placed into sample tubes, which were then compacted and sealed with paraffin film for 3 weeks to establish equilibrium for $^{210}Pb$ activities. Radioisotope analysis of the sub-samples was performed using an HPGe Gamma Spectrometer (ORTEC-GWL-120-15, EG&G, USA), with IAEA-RGU ore powder as the standard reference material. The specific activity of $^{210}Pb$ was calculated using the energy peak at 46.5 keV, and the specific activity of $^{226}Ra$ was calculated using the energy peaks of its progeny $^{214}Pb$ (351.9 keV) and $^{214}Bi$ (609.2 keV). The difference in specific activity between $^{210}Pb$ and $^{226}Ra$ represents the excess $^{210}Pb_{ex}$ specific activity. The statistical errors for $^{210}Pb$ and $^{226}Ra$ were <20% and <10%, respectively (at a 95% confidence level). The vertical distribution of excess $^{210}Pb$ specific activities was used to calculate the sedimentation rate and establish an age model for each core.

## 2.6 Lignin analyses

The sediment samples were subjected to the CuO oxidation method by Hedges and Ertel (1982) to extract lignin-derived phenol. First, 0.5 g of dry sediment and 1.0 g of CuO were weighed into a 25 mL Polytetrafluoroethylene (PTFE) reaction minibomb. In a glove bag filled with $N_2$, 10 mL of 2 M oxygen-free NaOH ($N_2$ was blown into the solution for 5 min) was added into the PTFE vessels. The PTFE vessels were placed in a muffle furnace and heated at 170°C for 3 h. The reaction vessels were then cooled. The solution was washed with 1 M NaOH and then placed in a 50 ml centrifuge tube and centrifuged. This step was repeated three times. The lignin in the supernatant was extracted three times using $C_4H_8O_2$ in a separator funnel. Anhydrous $Na_2SO_4$ was added to the extract to remove water, and the extract was filtered using filter paper. The extract solution was added, with 100 μL of ethyl vanillin as the internal standard, and then concentrated to 1–2 ml using a rotary evaporator. $N_2$ was blown into the remaining concentrated solution to dry the solution and obtain solid oxidation products. An equal volume of $C_5H_5N$ and $C_8H_{18}F_3NOSi_2$ with 10% $C_3H_9ClSi$ were added into the oxidation products and heated at 90°C for derivation purposes. Gas chromatography (GC-2010 Plus, SHIMADZU, Japan) was used to elucidate the lignin monomers. The heating procedure of the GC column was from 100°C to 300°C at a rate of 4°C $min^{-1}$. The concentration of each lignin phenol was determined based on the retention time of each lignin and the internal standard.

Lignin is a good indicator of terrigenous OM and is widely utilized in the environment of continental shelf, estuarine, lake, peatland, and salt marsh (Lourençato et al., 2019). Lignin phenol is one of the main components of plant-derived OM, which can indicate the vegetation composition of mangroves due to its unique biogeochemical characteristics (Lowman et al., 2021; Xia et al., 2023). The value of Λ6 is the sum of syringyl and vanillin phenols, whereas the value of Λ8 is the sum of Λ6 and cinnamyl phenols. The ratio of syringyl to vanillyl phenols (S/V) can be used to distinguish gymnosperms (S/V is approximately 0) and angiosperms (S/V > 0), and the ratio of cinnamyl to vanillyl phenols (C/V) can be used to distinguish woody (C/V is approximately 0) and non-woody (C/V > 0) tissues (Hedges and Mann, 1979). Furthermore, Tareq et al. (2004) proposed the lignin–phenol vegetation index (LPVI) to accurately determine the source of terrestrial OM; the ranges of LPVI values of the woody and non-woody tissues of gymnosperms are 1 and 12–17, respectively, and the ranges of LPVI values of woody and non-woody tissues of angiosperms are 67–415 and 378–2782, respectively. In addition, the acid–aldehyde ratios of syringyl [(Ad/Al)s] and vanillyl [(Ad/Al)s] phenols can be used to indicate the degree of lignin degradation under microbial action. In general, the (Ad/Al)s and $(Ad/Al)_V$ of fresh plant tissues were less than 0.14 and 0.3, respectively. If (Ad/Al)s is greater than 0.16 and (Ad/Al)v is greater than 0.6, lignin is considered to have undergone high degradation (Hedges et al., 1988).

## 2.7 Calculation of OC stocks

The OC storage in the sediment was calculated as follows: (1) dry bulk density ($D_{dry}$) is equal to the ratio of dry subsample mass ($M_{dry}$) to wet sample volume ($V_{wet}$) (Equation 1), (2) calculation of the amount of TOC based on TOC percentage and $D_{dry}$ of each layer (Equation 2), and (3) SOC storage is the ratio of the $TOC_{layer}$ of each layer to the cross-sectional area of each layer (Equation 3).

$$D_{dry}\ (g\ \ cm^{-3}) = M_{dry}\ (g)/V_{wet}\ (cm^3) \quad (1)$$

$$TOC_{layer}\ (g) = D_{dry}\ (g\ cm^{-3}) \times H\ (cm) \times A(cm^2) \times TOC(\%) \times 0.01 \quad (2)$$

$$SOC(Mg\ C_{org}\ ha^{-1}) = 100 \times TOC_{layer}\ (g)/A\ (cm^2) \quad (3)$$

where $M_{dry}$is the mass of 2 $cm^{-3}$ sub-sample after drying, $V_{wet}$ is 2 $cm^{-3}$, $H$ is the thickness of each sediment layer (2 cm), and $A$ is the cross-sectional area of the sample column (28.3 $cm^2$). $TOC_{layer}$ is the TOC content of each sediment layer (Supplementary Table S2).

## 2.8 Calculations of OM fractions

The sources of OM fractions in the forms of mangrove and terrestrial and marine fractions in the mangrove sediment were calculated using the SIMMR software package. The detailed calculation method and process of the SIMMR software package were described by Parnell and Inger (2016). The $\delta^{13}C$ and C/N values of mangrove leaves of different tree species in Qinzhou City (Guangdong Province) were used to represent the end-members of mangrove plants, in which the average value of $\delta^{13}C$ is -28.72 ± 0.78‰, and the average value of C/N is 37.41 ± 9.65 (Xia et al., 2015; Meng et al., 2016). As the collected data were exclusively obtained from mangrove forests in Guangxi, characterized by the same mangrove species, these data adequately represent the end-member value of mangrove OM. Xia et al. (2015) found that in areas with similar drainage and material sources, the C/N and $\delta^{13}C$ values of river sediments are generally same. Therefore, this study used the river $\delta^{13}C$ (-24.1 ± 0.6‰) and C/N (12.8 ± 2.1) data provided by Xia et al. (2015) as the end-member values for river OM. The average values of $\delta^{13}C$ and C/N of phytoplankton in the northern South China Sea of -16.10 ± 0.80‰ and 6.50 ± 0.10, respectively (Hou, 2009), were used as the end-members for phytoplankton OM fraction. The specific data and sources of each end-member value are shown in Supplementary Table S1.

## 2.9 Statistical analyses

Given that not all parameters conform to the normal distribution, the Mann–Whitney U test was used to compare the differences in measured parameters among different cores. The correlation between different parameters along the cores was determined using Spearman's correlation analysis. IBM SPSS Statistics software was used for statistical analysis of the data, and a $p$ value of 0.05 was used to determine its significance. Assessment of the significance of changes in C/N and $\delta^{13}C$ values in sediments were based on variance changes using the F-test (Sánchez et al., 2023). Origin Pro 2022b was used to draw and analyze the data. The *SIMMR* software package was used to establish an end-member mixing model based on C/N values and $\delta^{13}C$ value to analyze the relative contributions of different OM sources (Parnell et al., 2013).

# 3 Results

## 3.1 Sedimentation rates and age model

Based on the *SERAC* package provided by Bruel and Sabatier (2020), three models, namely, the constant flux constant sedimentation (CFCS), the constant initial concentration (CIC), and the constant rate of supply (CRS), were used to calculate the sedimentation rate and age patterns along the GX1 and GX2 cores. The total $^{210}Pb$ specific activity (75.82–179.67 Bq $kg^{-1}$) along the two cores is greater than that of $^{226}Ra$ (32.77–60.36 Bq $kg^{-1}$). The depth of the two cores, GX1 and GX2, has not reached the background value of $^{210}Pb$ in this area; thus, the CRS model is not applicable. In addition, the reliability of the calculated results of the CIC model is poor. Thus, the ages along the GX1 and GX2 cores were calculated using the CFCS model. The $^{210}Pb$ activity of GX1 has a high degree of linear fit ($r^2$ = 0.87) to the depth profile (Figure 2A). The pattern observed along GX2 is consistent with a stepped pattern of $^{210}Pb$ activity (Figure 2B); therefore, the age model along GX2 was divided into two parts, 0–71 and 71–95 cm, with a fit of 0.67 and 0.89, respectively. The mean sedimentation rate along GX1 was 17.7 ± 2.9 mm $yr^{-1}$, and the ages ranged between 1972 and 2021 (Figure 2A). The deposition rates along GX2 were 80 ± 22.4 and 17.3 ± 5.4 mm $yr^{-1}$ at 95–71 and 71–0 cm, and the corresponding ages were 1977–1980 and 1980–2021, respectively (Figure 2B).

## 3.2 Sediment grain size

The average grain size, sorting coefficient, kurtosis, and skewness of the sediments in the study area are 4.93±0.49, 2.28 ±0.18, 0.95±0.12, and 0.37±0.12, respectively, with the variation trends shown in Figures 3A–D. The following formula is used to calculate particle size. The larger the calculated φ value, the smaller the particle diameter D.

$$X\ (\varphi) = -2log_2(D) \quad (4)$$

where $X$ is the normalized particle size, and $D$ is the particle diameter. φ values decreased from 5.33 φ (in 1964) to 4.74 φ (in 2001) along GX1 and decreased from 5.99 φ (in 1963) to 4.64 φ (in 2001) along GX2 (Figure 3A), indicating increased particle size from around 1963 to 2001. No evident change was observed in the trend of average particle size along both cores from 2000 to 2020. According to the Shepard method (Shepard, 1954), three lithologies exist in the GX1 and

10.3389/fmars.2024.1410183

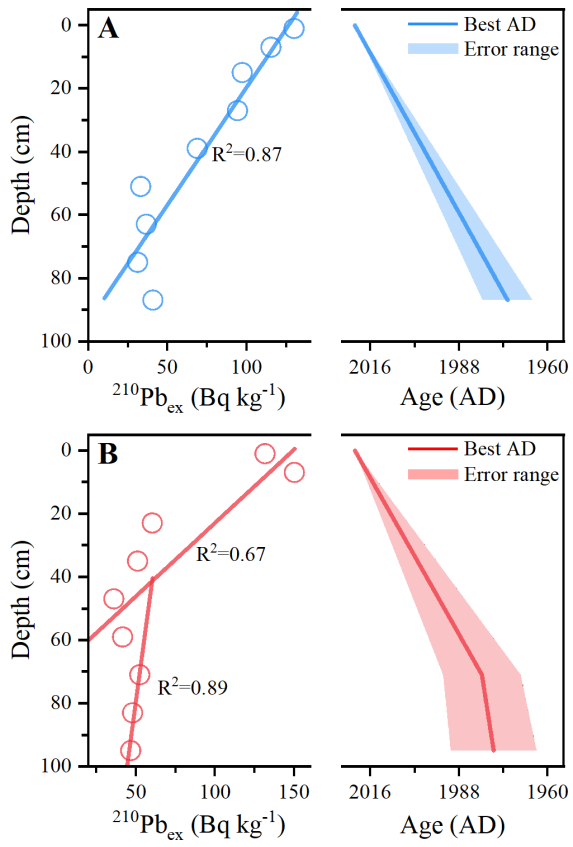


FIGURE 2
Linear fitting of $^{210}$Pb radioisotope results and age-depth models of cores **(A)** GX1 and **(B)** GX2, where the blue and red lines represent the best age, and the blue and red areas represent the margin of error in the calculation of the chronology model.

GX2 sites (Figure 4A): silty-sand, sandy-silt, and clayey-silt. Both GX1 and GX2 showed a silty-sand type (more sand) in the surface layer and a sandy-silt type (more silt) in the deeper layer. Averages of 39.31% ± 14.32% sand, 47.43% ± 12.25% silt, and 13.27% ± 2.87% clay were found throughout 1963–2001 along both sediment cores, and 50.87% ± 5.46% sand, 36.39% ± 4.04% silt, and 12.74% ± 1.76% clay were observed throughout 2001–2020 (Figure 4B).

## 3.3 Bulk elemental composition (TOC and TN) and $\delta^{13}$C value

The percentages of TOC and TN values along both cores ranged from 0.39% to 2.05% and 0.026% to 0.093%, respectively. The mean content of TN along GX1 and GX2 was the same at 0.05%; however, the average content of TOC in GX1 (1.23%) was slightly higher than that of GX2 (1.15%). The molar ratio of TOC/TN ranged from 15 to 30 (Supplementary Table S2). The C/N values of GX1 remained at approximately 25 from 1963 to 2001, but decreased from 25 to 15 from 2001 to 2020, which was significant ($F_{8,14,\ \alpha=0.05}$ = 3.49). The C/N ratio along GX2 also showed a noticeable decrease, but this change is not significant. Stable carbon isotope ratios ($\delta^{13}$C) ranged from -27.21‰ to -25.65‰ (Supplementary Table S2).

TOC content along GX1 and GX2 showed a slight decreasing trend from 1963 to 2020, whereas TN content remained stable from 1963 to 2010 and increased slightly from 2010 to 2020 (Figures 5A, B). From 1963 to 2001, the mean $\delta^{13}$C values of GX1 and GX2 were -26.50‰ and -26.68‰, respectively. From 2000 to 2020, the $\delta^{13}$C values of GX1 and GX2 increased from -26.50‰ to -25.65‰ and from -26.68‰ to -25.82‰, respectively (Figures 5C, D). The variation in $\delta^{13}$C values along GX1 was significant ($F_{8,14,\ \alpha=0.05}$ = 3.32), whereas there is no significant variation along GX2.

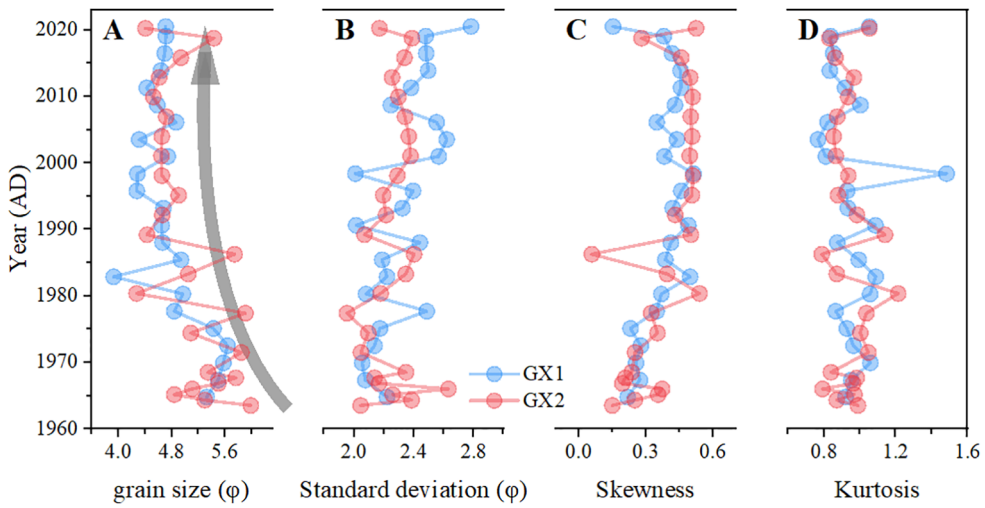


FIGURE 3
**(A)** Mean grain size, **(B)** standard deviation, **(C)** skewness, and **(D)** kurtosis along the vertical profile of the cores GX1 (represented by solid blue circles, of which the ages along the core span from 1964 to 2020) and GX2 (represented by solid pink circles, of which the ages along the core span from 1963 to 2020).

10.3389/fmars.2024.1410183

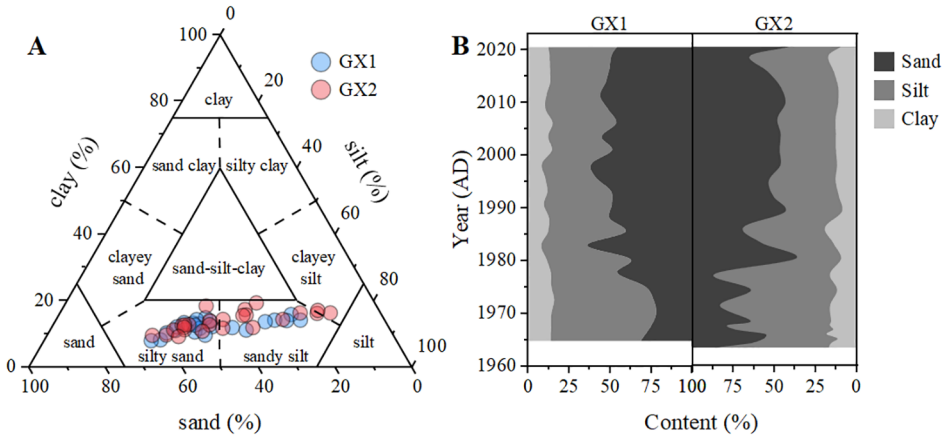


FIGURE 4
**(A)** Categories of particle size among each subsample according to the Shepard method (1954); **(B)** The clay, silt, and sand grain contents along the depths of cores GX1 and GX2.

## 3.4 Three end-member mixing model and potential sources of OM

The proportions of MOM, river OM and marine OM along the GX1 sediment core were 63.08% ± 6.73%, 26.36% ± 6.12% and 10.58% ± 0.95%, respectively. The proportions of MOM, river OM and marine OM along the GX2 sediment core were 63.99% ± 7.30%, 25.64% ± 6.15% and 10.36% ± 1.27%, respectively. In summary, the proportions of MOM, river OM and marine OM in GX1 and GX2 sediment accounted for 63.56% ± 7.05%, 25.98% ± 6.14% and 10.46% ± 1.13% of the total OM, respectively (Supplementary Table S3). In the early stages of sediment deposition (1963–2001), MOM, river OM and marine OM accounted for approximately 65.73% ± 3.04%, 23.76% ± 2.35% and 10.52% ± 0.88% of total OM, respectively. In the following stage of sediment deposition (2001–2020), MOM, river OM and marine OM accounted for approximately 57.34% ± 7.52%, 31.50% ± 6.66% and 11.16% ± 1.21% of the total OM, respectively.

## 3.5 Lignin

The value of Λ6 is the sum of syringyl and vanillin phenols, whereas the value of Λ8 is the sum of Λ6 and cinnamyl phenols. The average values of Λ6 and Λ8 in GX1 were 4.60 ± 1.00 and 4.94 ± 1.07 mg/100 mg OC, whereas in GX2, the values were 5.20 ± 1.31 and 5.66 ± 1.43 mg/100 mg OC. The trend of total lignin content Λ6 and Λ8 remains basically the same (Figures 6A, B; Spearman's rho = 0.997, $p < 0.001$). The S/V and C/V ratios of GX1 ranged from 0.82–1.03

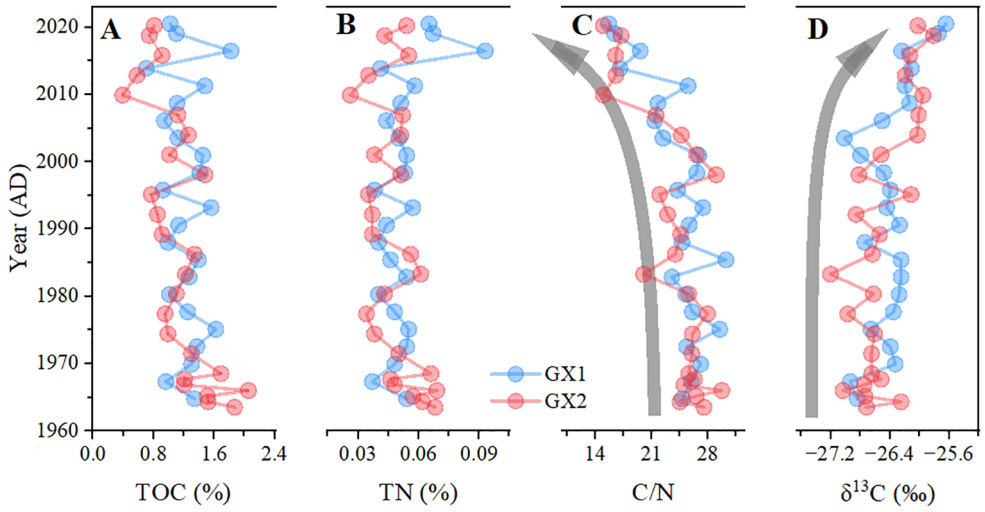


FIGURE 5
**(A)** Total organic carbon (TOC), **(B)** total nitrogen (TN), **(C)** carbon/nitrogen (C/N) ratio, and **(D)** stable isotope signature ($\delta^{13}C$) along the vertical profile along cores GX1 and GX2 (solid blue circles represent GX1, the core was from 1964 to 2020; solid pink circles represent GX2, the core was from 1963 to 2020).

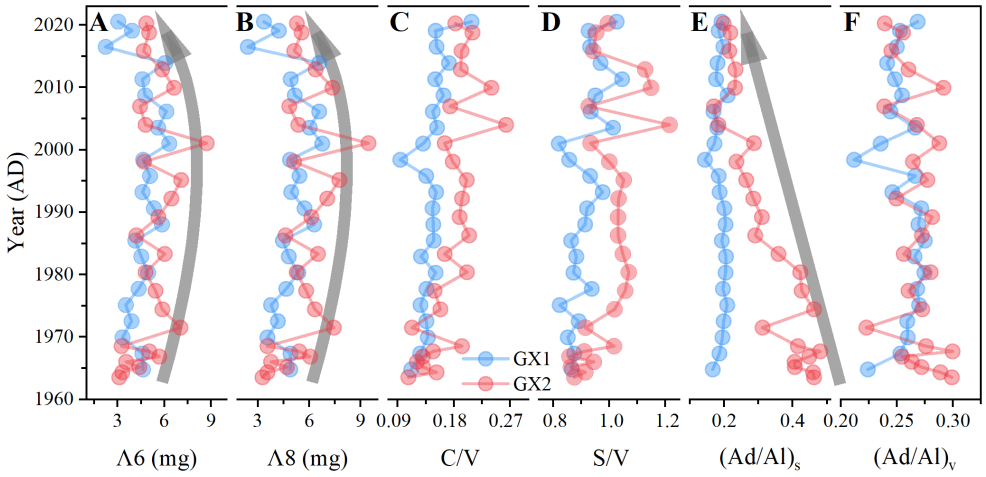


FIGURE 6
The ratios of **(A)** cinnamyl to vanillyl phenols (C/V), **(B)** syringyl to vanillyl phenols (S/V), **(C)** acid to aldehyde of syringyl phenols, $(Ad/Al)_s$, and **(D)** acid to aldehyde of vanillyl phenols $(Ad/Al)_v$; and sum of **(E)** total monomers of vanillyl and syringyl phenols (Λ6) and **(F)** total monomers of vanillyl, syringyl, and cinnamyl phenols (Λ8).

(mean 0.92 ± 0.06) and 0.09–0.21 (mean 0.14 ± 0.02), respectively. The S/V and C/V ratios of GX2 ranged from 0.86–1.21 (mean 0.99 ± 0.09) and 0.11–0.26 (mean 0.17 ± 0.04), respectively. The LPVI values of GX1 and GX2 were 876–3279 and 1091–8038, with an average of 1727 and 2771, respectively. The (Ad/Al)s and (Ad/Al)v were 0.14–0.21 (mean 0.19 ± 0.02) and 0.21–0.27 (mean 0.26 ± 0.02) along GX1 and 0.17–0.48 (mean 0.33 ± 0.10) and 0.22–0.30 (mean 0.27 ± 0.02) along GX2, respectively (Supplementary Table S4). The Mann–Whitney U test results showed significant differences in C/V values ($p = 0.003$) and S/V values ($p = 0.003$) between GX1 and GX2 sites. The results of the Mann–Whitney U test showed significant differences in (Ad/Al)s ($p < 0.001$) and (Ad/Al)v ($p = 0.043$) values between the GX1 and GX2 samples.

Total lignin content increased slightly from 1964 to 2000 but decreased from 2000 to 2020 (Figures 6C, D). No significant change is observed in the (Ad/Al)s of GX1 from the bottom to the surface sediment; however, a significant decrease in (Ad/Al)s from the bottom to surface of core GX2 is observed. The (Ad/Al)v values of GX1 and GX2 did not change significantly from the bottom to the top of the sediment (Figures 6E, F). The values of C/V (Spearman's rho = 0.662 to 0.704, $p < 0.001$) and S/V (Spearman's rho = 0.482 to 0.633, $p < 0.015$) showed a significant positive correlation with age at GX1 and GX2. (Ad/Al)s value (Spearman's rho = 0.893, $p < 0.001$) was significantly negatively correlated with age at GX2, whereas the (Ad/Al)s value of GX1 did not change significantly with age.

# 4 Discussion

## 4.1 Sedimentary organic carbon stocks and sources

Mangrove forests store a remarkable amount of OC in the sediments. In the current study, the OC stock in the one-meter-top sediments is estimated to be an average of 144.5 Mg $C_{org}$ $ha^{-1}$. The estimation aligns closely with the estimated SOC stock in the 8-year-old restored mangrove forests at the Shijiao station of Pearl Bay; however, this value is lower than the natural mangrove forests (Figure 6.5 in Chen et al., 2021). Integrating these results indicates that the average SOC stock in the mangrove forests of Pearl Bay is approximately 150 Mg $C_{org}$ $ha^{-1}$. This figure is notably lower than the national average for China, which is reported as 270.39 ± 76.25 Mg $C_{org}$ $ha^{-1}$ (Liu et al., 2014) and the global average of 334 Mg $C_{org}$ $ha^{-1}$ (Kauffman et al., 2020). Such comparisons suggest that the mangrove forests in Pearl Bay possess a comparatively diminished capacity for carbon storage. Various factors, both biotic and abiotic, influence the carbon storage capacity of mangrove forests. Notably, temperature always emerges as a primary abiotic factor governing the spatial pattern of SOC stock (Kauffman et al., 2020; Wang et al., 2021). Recently, tidal range has been identified as a critical driver of carbon storage (Wang et al., 2021). Compared to previously published results, the average SOC stock in our study is similar to the area with a similar temperature condition within the meso-tidal range of 2–4 m, which is lower than the area with a micro-tidal range of 0–2 m (Supplementary Figure S1). The average SOC value of six micro-tide areas was 304.68 Mg $C_{org}$ $ha^{-1}$ (Cai et al., 2013; Feng et al., 2019; Gao et al., 2019; Wang et al., 2019; Peneva-Reed et al., 2021; Rovai et al., 2021), and the average SOC value of six meso-tide areas was 137.23 Mg $C_{org}$ $ha^{-1}$ (Bhomia et al., 2016; Palacios Peñaranda et al., 2019; Wang et al., 2019; Su et al., 2020; Bacar et al., 2023). Lower tidal ranges can reduce mangrove contact time with the tide, thus reducing the likelihood of SOC being washed away and retaining more SOC (Wang et al., 2021). Perera and Amarasinghe (2019) also found that mangrove sediment in Sri Lanka have a better carbon sequestration function under a micro-tide environment, and the SOC sequestration capacity is significantly negatively correlated with the average tidal amplitude. Furthermore, lower SOC may have attributed to a faster rate of SOC decomposition in areas with larger tidal ranges and more frequent tidal inundation due to the frequent renewal of electron

acceptors, which may lead to a lower degree of OC preservation and lower OC stock in sediments (Marchand et al., 2004, 2006).

In areas with similar temperatures and tidal ranges (approximately 2.4 m), we found that the SOC of mangroves in Pearl Bay is also significantly lower than that of Gaoqiao (260.3 Mg $C_{org}$ $ha^{-1}$), Yingluo Bay (237.68 Mg $C_{org}$ $ha^{-1}$) and Zhanjiang (202.7 Mg $C_{org}$ $ha^{-1}$) mangroves (Wang et al., 2013; Gao et al., 2019; Yan et al., 2024). We hypothesize that the rate of sediment increase is another key factor and that faster sedimentation rates lead to lower SOC content. Higher sedimentation rates suggest that mangroves may have received more input from inland sediments, which tend to contain more mineral sediment, thus diluting the OC content (Kusumaningtyas et al., 2019). Therefore, when deposited to the same depth, a high deposition rate corresponds to low carbon storage, which is confirmed by the fact that the deposition rate of Yingluo Bay and Gaoqiao (6.5–11 mm $a^{-1}$) sediments is lower than that of Pearl Bay (17.5 mm $a^{-1}$) (Zhu et al., 2016).

Previous studies have shown that OC decomposition is constrained by the composition of OC because the residues of different plants have different resistance to decomposition (Hemminga and Buth, 1991; Valéry et al., 2004). Sedimentary OC in mangrove forests is a composite of autochthonous inputs, including above ground biomass (e.g., leaves and branches) and below ground biomass (e.g., fine roots), as well as allochthonous inputs from river and marine environments (Krauss et al., 2014; Stringer et al., 2016; Xiong et al., 2018b; Sasmito et al., 2020). The SOC in salt marsh ecosystems primarily relies on its combination with fine-grained minerals to form mineral OC, whereas SOC in mangrove forests mainly depends on high aromaticity and low mineral OC (Sun et al., 2019). Therefore, we consider that the decomposition rate of MOM is lower than that of allochthonous OM in mangrove sediments. Under such a mechanism for carbon fixation, nitrogen content can significantly affect the decomposition rate of OM, and OM with a higher C/N value has stronger resistance to biodegradation (Jones et al., 2016). MOM from mangrove vegetation has a higher C/N value and a high refractory compound content, such as tannins, lignin, and cellulose (Holmer and Olsen, 2002; Friesen et al., 2018). In contrast, allochthonous OM from river or marine environments are relatively more susceptible to degradation due to their high nitrogen content. The high C/N (23.74±4.06‰), C/V (0.96 ± 0.09), S/V (0.16 ± 0.03), and lower $\delta^{13}C$ value (-26.45±0.35‰) in the study area indicate that the organic matter is primarily derived from local $C_3$ mangrove angiosperms (Figures 7A, B). This finding was consistent with the output of the *SIMMR* model showing that MOM accounted for 63.56% ± 7.05%, river OM accounted for 25.98 ± 6.14% and that marine OM accounted for 10.46% ± 1.13% of the total sedimentary OM. Based on Figures 8A, B, the decrease in river and marine OM with increasing depth aligns with the hypothesis of preferential degradation of river and marine OM. In regions with similar temperatures, we also observed a high proportion of MOM in the sediments. For instance, in Yingluo Bay, the C/N ratios varied from 12.3 to 25.0, with the $\delta^{13}C$ values from -28.8‰ to -26.6‰ and 67.0%–88.1% autochthonous input (Xia et al., 2015). On Qi'ao Island, the C/N ratios ranged from 12.032 to 26.690, with a 70.21% autochthonous input (Jiang et al., 2021). Among the three investigated regions, Pearl Bay demonstrated the lowest concentration of MOM, thereby leading to lower SOC levels (150 Mg $C_{org}$ $ha^{-1}$) relative to Yingluo Bay (237.68 Mg $C_{org}$ $ha^{-1}$) and Qi'ao Island (210.62 Mg $C_{org}$ $ha^{-1}$) (Xia et al., 2015; Jiang et al., 2021). Similar findings were reported by Suello et al. (2022) in the mangroves of Ecuador, where mangrove forests with high inputs of MOM exhibit relatively higher SOC content.

As one of the main components of plant-derived OM, lignin is also widely used to trace OM in continental shelves, estuaries, lakes, and other environments (Lourençato et al., 2019; Lowman et al., 2021; Xia et al., 2023). The Λ8 value of this study is 5.31 mg/100 mg TOC, whereas the Λ8 value of general mangrove sediment is 1.05–6.78 mg/100 mg TOC, and the Λ8 value of estuarine sediment is 0.36–1.87 mg/100 mg TOC, which provides additional confirmation of the relatively high MOM input in mangroves (Li et al., 2017). The S/V and C/V ratios range from 0.82 to 1.21 (Avg. 0.96 ± 0.09) and 0.09 to 0.26 (Avg. 0.16 ± 0.03), respectively. These values indicate that OM in the sediments primarily originated from the non-woody tissues of angiosperms, which is consistent with the LPVI values, ranging from 876 to 8083, with an average of 2271 ±

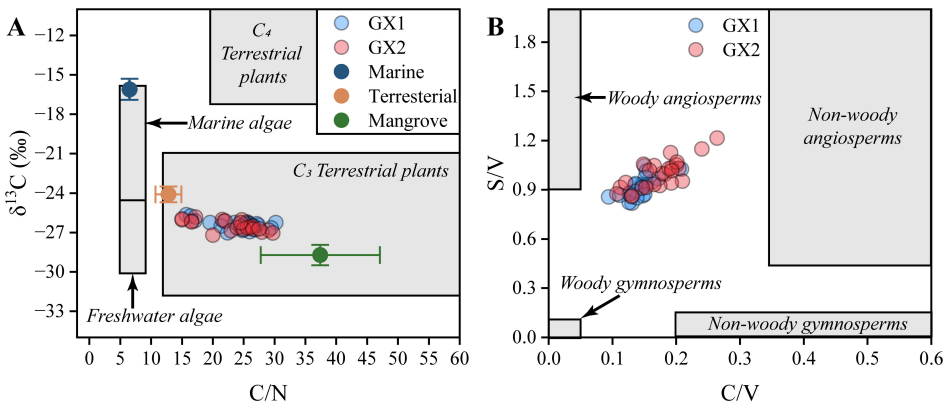


FIGURE 7
**(A)** Scatter plot of $\delta^{13}C$ and C/N for all sediment samples. The gray area borders are based on Lamb et al. (2006). **(B)** Scatter plot of C/V values and S/V values for all sediment samples. The gray area borders are based on Jex et al. (2014).

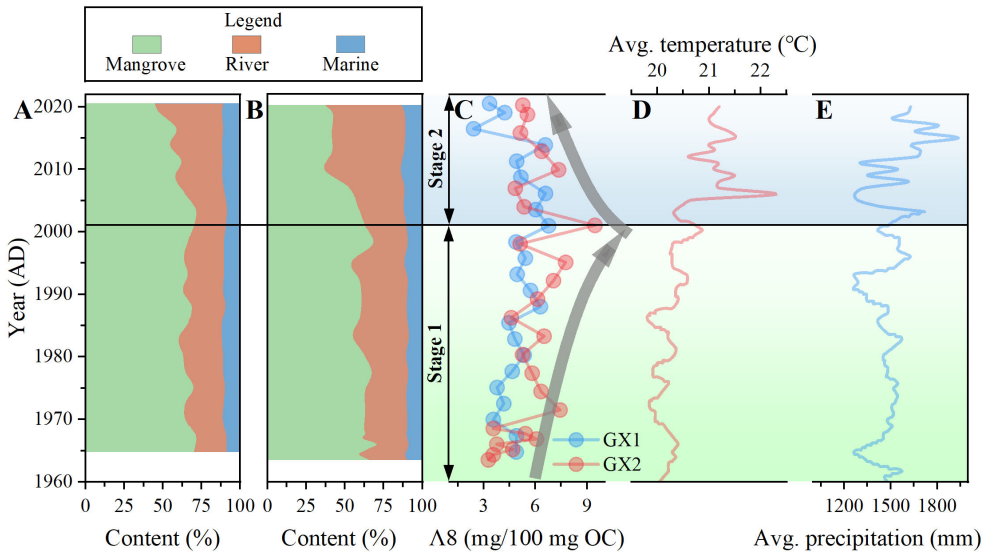


FIGURE 8
Changes in the proportion of organic matter (OM) contributions from mangrove and allochthonous sources in GX1 **(A)** and GX2 **(B)** mangrove soil; **(C)** Total lignin content of GX1 and GX2; **(D)** Annual average air temperate and **(E)** precipitation recorded by Guangxi Climate Center (Huang et al., 2007); Stage 1 (green area) and stage 2 (blue area) represent the periods of growth and degradation, respectively, in **(C–E)**.

1308. Considering that only mangrove plants exist in the vicinity of the sampling points, these non-woody tissues of angiosperms mainly derive from mangrove leaves. Similar mixed signals were found in the surrounding area. For example, the C/V and S/V values range from 0.09–0.18 and 0.82–1.02 in Bamen Bay, Hainan (Bao et al., 2013b). Compared with Ad/Al values of fresh plants, only syringyl phenols have degraded a small part in mangrove sediments, whereas vanillyl phenols have almost not degraded, which indicates that lignin in mangrove sediments in Pearl Bay is well preserved (Hedges et al., 1988). This finding also confirms the hypothesis mentioned earlier that a large input of MOM leads to slower decomposition and enhances its preservation, thereby increasing SOC content. The same situation was found in Guangxi, Guangdong, and Hainan, where lignin in sediments was basically not degraded. In the Pearl River Estuary and Shenzhen Bay, the (Ad/Al)s value is 0.16, and the (Ad/Al)v value ranges from 0.16 to s0.22 (Zhao et al., 2023). Another possible reason for the excellent preservation of lignin could be attributed to the comparatively higher rate of sedimentation. The half-life of lignin in mangrove leaf litter is 150–300 years (Dittmar and Lara, 2001). In addition, the high deposition rate causes the surface sediments to be rapidly buried in an anaerobic environment, and the lignin is more difficult to decompose.

## 4.2 Reasons for the changes in C/N and $\delta^{13}C$ values

Although the decomposition rate of OM in sediments is relatively slow in mangrove ecosystems, it still causes changes in C/N and $\delta^{13}C$ values in sediment cores (Dittmar and Lara, 2001). Sampling sites GX1 and GX2 are located near the estuary, where sediment distribution is influenced by multiple disturbances such as sea level rise and human activities. These factors may enhance the degradation potential of OM in the sediments (Jonge et al., 2015). As shown in Figures 3A and 4B, the sediment particle size gradually increases from the bottom to the top of the core, which indicates that the sedimentary environment of the sampling point has changed from a silt sedimentary environment (weak tidal action) to a sand sedimentary environment (strong tidal action). In a sand sedimentary environment, the inability of coarse particles to effectively encapsulate OM and prevent its decomposition, combined with the aforementioned strong tidal action, leads to a faster rate of OM degradation (Sanders et al., 2012). However, if the OM input source remains unchanged, Figure 9A indicates that the carbon stock increases with sediment age, which contradicts the theory of organic OM degradation. Cui et al. (2021) noted that due to the high content of recalcitrant carbon, such as lignin, in MOM, the decomposition of fresh litter leads to an initial increase followed by a decrease in the proportion of labile OC in the sediment. Figure 5A shows that the OC content continues to increase with age, which does not conform to the theory proposed by Cui et al., indicating that the degradation of OM in the sediments cannot explain this trend. Yan et al. (2023) pointed out that the degradation of sediment OM leads to an increase in $\delta^{13}C$ values and a decrease in the C/N ratio. However, the trends shown in Figures 5C, D are contrary to this. Moreover, if significant degradation of OM were occurring, TOC and TN values would decrease with the increasing age of the sediments. However, Figures 5A, B clearly do not show this trend. Correlation tests showed that the total lignin content is significantly correlated with TOC and TN ($p < 0.001$), which indicated that the degree of degradation of OC may be the same as that of lignin. However, the (Ad/Al)s and (Ad/Al)v values showed that lignin is basically not degraded and that the total

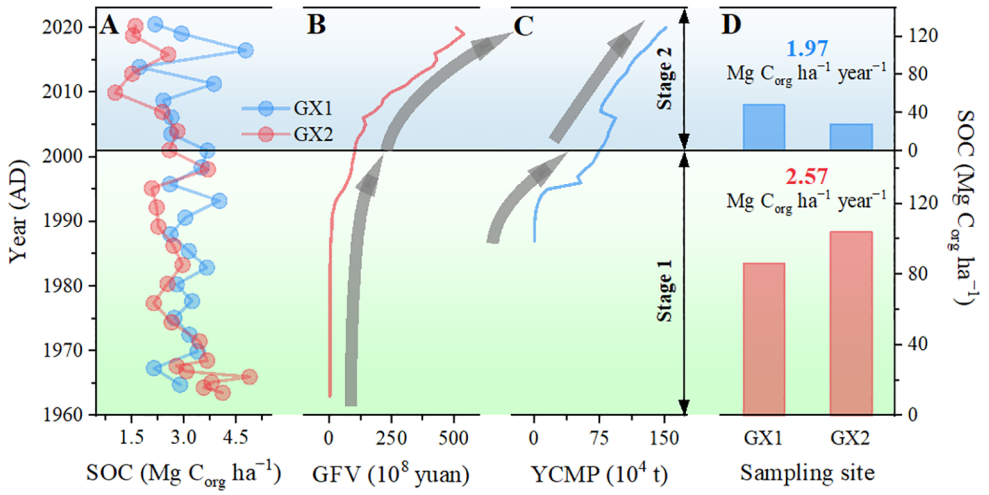


FIGURE 9
**(A)** Vertical profile of soil organic carbon (SOC) along the GX1 and GX2 core; **(B)** gross fishery value of Guangxi and **(C)** yield of cultured marine products in Guangxi (cited from 2022 Guangxi Statistical Yearbook, http://tjj.gxzf.gov.cn//tjsj/tjnj/material/tjnj20200415/2022/zk/indexch.htm); **(D)** Core OC storage and accumulation rate for both stages 1 and 2; stage 1 (green area) and stage 2 (blue area) represent the periods of growth and degradation, respectively.

lignin content in the surface layer of the sediment increases with increasing depth. This trend further confirms that OM has not undergone significant degradation. Under the condition of constant sedimentation rates and well-preserved OM in surface sediments, an increase in SOC with depth indicates an increase in the OC content of the OM. Therefore, the degradation of OM in the surface sediment of the sampling point is not the main reason for the change of C/N and $\delta^{13}C$ values, but is more likely to be caused by the change in OM input source. Because OM from riverine and marine environments has a lower C/N ratio and higher $\delta^{13}C$ values (Figure 7A), whereas mangrove OM has a higher C/N ratio and lower $\delta^{13}C$ values (Lamb et al., 2006), and considering the trends of the lignin parameters, the trends observed in Figures 5C, D may be attributed to a decrease in MOM input.

## 4.3 Response of mangrove carbon sinks to external factors

In the previous section, we excluded the factor of OM degradation. The damage to mangroves caused by climate change-induced sea level rise or increased intensity of human activities may also lead to the loss of OC in sediment (Bozi et al., 2021; Wang and Gu, 2021). Sea level rise increases tidal height and the frequency of seawater intrusion into the mangrove, which affects the sources of OM and carbon storage in mangrove sediments (Perera et al., 2018; Wang et al., 2019). As shown in Figures 8A–C a gradual decrease in MOM and total lignin content is observed from the bottom to the top of the core. The lack of a clear pattern in local precipitation and temperature variations suggests that these factors may not be the primary influences (Figures 8D, E). While the enhanced tidal effects resulting from sea level rise may contribute to this trend, we consider that this is not the primary reason. This is because the average sediment deposition rate in the study area is 17.5 mm a$^{-1}$, which is much higher than the sea level rise rate of Pearl Bay (2 mm aa$^{-1}$), indicating that the salinity and tidal inundation frequency of mangrove habitats remain largely unaffected, as also found in Ellison (2008) and Ma et al. (2022). Xia et al. (2019) also proposed that when the sediment deposition rate (4.4 mm a$^{-1}$) is higher than the sea level rise rate, the change of sediment OM source exhibits a minimal relationship with sea level rise. Li et al. (2015) established a vulnerability assessment index system for coastal mangroves in response to sea level rise and indicated that the mangroves in Pearl Bay, Guangxi, have shown non-vulnerability in the face of sea level rise. This also supports the opinions of our study. Since sea level rise is not the primary factor threatening mangroves, we hypothesize that the changes in parameters are due to mangrove degradation caused by human activities, leading to a decrease in the input of native OM. Based on the changing trends in the sources of OM, the anthropogenic activities in the sedimentary record can be divided into two distinct stages: 1963–2001 and 2001–2020. In stage 1 (1963–2001), mangroves were less affected by human activities, thereby ensuring a consistent supply of MOM. However, in stage 2 (2001–2020), the mangroves may have experienced a certain degree of degradation due to frequent human activities, leading to a gradual reduction in the provision of MOM. The decline in the rate of SOC accumulation (Figures 9A, D) from 2.57 Mg $C_{org}$ ha$^{-1}$ yr$^{-1}$ (stage 1) to 1.97 Mg $C_{org}$ ha$^{-1}$ yr$^{-1}$ (stage 2) implies mangrove forest degradation. As the lignin in the sampling locations is exclusively derived from fresh mangrove tissues (Bao et al., 2013a), the declining trend in total lignin content from 2001 to 2020 provides additional support for our hypothesis (Figure 8C). In pursuit of economic growth, coastal regions have extensively converted mangrove wetlands into shrimp farming ponds. As a result, fishery-related economic indicators are employed as proxies for the intensity of human activities. Based on the variations in gross

fishery value (Figure 9B) and the yield of cultured marine products (Figure 9C), during the second phase, a substantial increase in human activity intensity is the primary cause of mangrove degradation. In addition, in 2011, a marine aquaculture system was established underneath the mangrove forest in the study area. Ouyang and Guo (2016) proposed that establishing a mangrove-aquaculture coupling system in mangrove areas can effectively treat wastewater generated by aquaculture, while the wastewater can provide essential nutrients for the growth and development of mangroves. However, this requires strict regulation of the scale of aquaculture. If wastewater discharge exceeds the limit, it can lead to eutrophication of the mangrove area, adversely affecting the growth of mangroves. While this aquaculture facility does not directly occupy the land within the mangrove forest, the discharge of aquaculture wastewater may induce changes in the physical and chemical properties of the surface sediment, ultimately leading to a loss of sediment carbon storage in the mangrove forest (Fan et al., 2013; Santos-Andrade et al., 2021).

The degradation of mangroves must be taken seriously, as the destruction of mangroves not only leads to a decrease in the OC deposition rate but also accelerates the decomposition of stored carbon in sediments, releasing greenhouse gases into the atmosphere. Ultimately, this could transform mangroves from a carbon sink into a carbon source (Senger et al., 2021). The effects of human activities on the mangroves in the study area are expected to gradually decrease in the future. This is evident from the inclusion of blue carbon conservation in the national strategy since 2015 and the introduction of the "Special Action Plan for Mangrove Conservation and Restoration (2020–2025)" in 2020 (Feng et al., 2024). However, whether the changes in temperature and precipitation patterns caused by climate change will pose a threat to the development of Pearl Bay mangroves remains uncertain. Currently, the observed changes in temperature and precipitation do not correspond well to the variations in parameters within mangrove sediments (Figures 8D, E). Therefore, these relationships must be investigated in future studies.

## 5 Conclusion

The results from this study indicate that under similar temperature conditions, mangrove with lower tidal ranges, slower sedimentation rates, and OM source primarily from mangrove plants store larger SOC. Additionally, based on the changes in lignin, we found that the decrease in MOM from the bottom to the top of the sediment core is not due to OM decomposition but rather the result of mangrove degradation. This degradation is likely caused by the increased intensity of human activities in the study area. Although mangroves can adapt to environmental pressures through various mechanisms, such as increasing sediment deposition rates to cope with sea level rise and absorbing nutrients from aquaculture wastewater to promote growth, their ability to regulate may become ineffective if environmental pressures increase too rapidly. In the future, due to the relatively low threat of sea-level rise to mangroves in the study area and the increased emphasis on mangrove protection in China, which has reduced the impact of human activities, it is expected that mangrove degradation will recover. We consider that stable lignin biomarkers can be used to assess the development of mangroves in other regions, allowing for the identification of the degree of mangrove degradation, followed by the implementation of timely measures to prevent carbon stock loss. This is crucial for using mangrove carbon storage to mitigate the negative impacts of climate change and human activities.

## Data availability statement

The original contributions presented in the study are included in the article/Supplementary Material. Further inquiries can be directed to the corresponding author.

## Author contributions

CG: Formal analysis, Investigation, Methodology, Writing – original draft. PL: Conceptualization, Resources, Supervision, Validation, Writing – review & editing. JH: Validation, Writing – review & editing. ZC: Investigation, Writing – review & editing. SP: Conceptualization, Resources, Validation, Writing – review & editing. CO: Conceptualization, Resources, Validation, Writing – review & editing. TS: Resources, Validation, Writing – review & editing. CM: Conceptualization, Resources, Validation, Writing – review & editing. CL: Conceptualization, Resources, Validation, Writing – review & editing. CB: Resources, Validation, Writing – review & editing. XL: Writing – review & editing. GA: Writing – review & editing. SK: Writing – review & editing. JW: Writing – review & editing.

## Funding

The author(s) declare financial support was received for the research, authorship, and/or publication of this article. This work was supported by Asia-Pacific Network for Global Change Research (APN) (Grant number: CRRP2020-06MY-Loh) and Ministry of Higher Education Malaysia for the HICoE Phase II fund (HICoE IOES-2023C).

## Acknowledgments

The authors acknowledge the Asia-Pacific Network for Global Change Research (Grant number: CRRP2020-06MY-Loh) and everyone who provided assistance during field trips.

## Conflict of interest

The authors declare that the research was conducted in the absence of any commercial or financial relationships that could be construed as a potential conflict of interest.

## Publisher's note

All claims expressed in this article are solely those of the authors and do not necessarily represent those of their affiliated organizations, or those of the publisher, the editors and the reviewers. Any product that may be evaluated in this article, or claim that may be made by its manufacturer, is not guaranteed or endorsed by the publisher.

## Supplementary material

The Supplementary Material for this article can be found online at: https://www.frontiersin.org/articles/10.3389/fmars.2024.1410183/full#supplementary-material

## References


Adame, M. F., Reef, R., Santini, N. S., Najera, E., Turschwell, M. P., Hayes, M. A., et al. (2021). Mangroves in arid regions: Ecology, threats, and opportunities. *Estuar. Coast. Shelf Sci.* 248, 1–9. doi: 10.1016/j.ecss.2020.106796

Alongi, D. M. (2014). Carbon cycling and storage in mangrove forests. *Annu. Rev. Mar. Sci.* 6, 195–219. doi: 10.1146/annurev-marine-010213-135020

Alongi, D. M. (2015). The impact of climate change on mangrove forests. *Curr. Clim. Change Rep.* 1, 30–39. doi: 10.1007/s40641-015-0002-x

Alongi, D. M. (2021). "Responses of mangrove ecosystems to climate change in the Anthropocene," in *Mangroves: Ecology, biodiversity and management*. Eds. i.P. Rastog, M. Phulwaria and D. K. Gupta (Springer Nature Singapore Pte Ltd, Singapore), 201–224.

Arias-Ortiz, A., Masqué, P., Glass, L., Benson, L., Kennedy, H., Duarte, C. M., et al. (2020). Losses of soil organic carbon with deforestation in mangroves of Madagascar. *Ecosystems* 24, 1–19. doi: 10.1007/s10021-020-00500-z

Atwood, T. B., Connolly, R. M., Almahasheer, H., Carnell, P. E., Duarte, C. M., Ewers Lewis, C. J., et al. (2017). Global patterns in mangrove soil carbon stocks and losses. *Nat. Clim. Change* 7, 523–528. doi: 10.1038/nclimate3326

Bacar, F. F., Lisboa, S. N., and Sitoe, A. (2023). The mangrove forest of quirimbas national park reveals high carbon stock than previously estimated in southern Africa. *Wetlands* 43. doi: 10.1007/s13157-023-01707-1

Bao, H., Wu, Y., Tian, L., Zhang, J., and Zhang, G. (2013a). Sources and distributions of terrigenous organic matter in a mangrove fringed small tropical estuary in South China. *Acta Oceanol. Sin.* 32, 18–26. doi: 10.1007/s13131-013-0295-3

Bao, H., Wu, Y., Unger, D., Du, J., Herbeck, L. S., and Zhang, J. (2013b). Impact of the conversion of mangroves into aquaculture ponds on the sedimentary organic matter composition in a tidal flat estuary (Hainan Island, China). *Cont. Shelf Res.* 57, 82–91. doi: 10.1016/j.csr.2012.06.016

Bhomia, R. K., MacKenzie, R. A., Murdiyarso, D., Sasmito, S. D., and Purbopuspito, J. (2016). Impacts of land use on Indian mangrove forest carbon stocks: Implications for conservation and management. *Ecol. Appl.* 26, 1396–1408. doi: 10.1890/15-2143

Blott, S. J., and Pye, K. (2001). GRADISTAT: a grain size distribution and statistics package for the analysis of unconsolidated sediments. *Earth Surf. Processes Landforms* 26, 1237–1248. doi: 10.1002/esp.261

Bouillon, S., Borges, A. V., Castañeda-Moya, E., Diele, K., Dittmar, T., Duke, N. C., et al. (2008). Mangrove production and carbon sinks: A revision of global budget estimates. *Global Biogeochem. Cycles* 22, 1–12. doi: 10.1029/2007gb003052

Bozi, B. S., Figueiredo, B. L., Rodrigues, E., Cohen, M. C. L., Pessenda, L. C. R., Alves, E. E. N., et al. (2021). Impacts of sea-level changes on mangroves from southeastern Brazil during the Holocene and Anthropocene using a multi-proxy approach. *Geomorphology* 390, 107860. doi: 10.1016/j.geomorph.2021.107860

Bruel, R., and Sabatier, P. (2020). serac: an R package for ShortlivEd RAdionuclide chronology of recent sediment cores. *J. Environ. Radioact.* 225, 106449. doi: 10.1016/j.jenvrad.2020.106449

Bunting, P., Rosenqvist, A., Hilarides, L., Lucas, R. M., Thomas, N., Tadono, T., et al. (2022). Global mangrove extent change 1996–2020: global mangrove watch version 3.0. *Remote Sens.* 14, 3657. doi: 10.3390/rs14153657

Cai, Y., Yanbo, J., Zhicheng, Z., Ruiping, C., Fei, Z., and Yinying, W. (2013). Sedimentary organic carbon dynamics in mangrove soil in shenzhen bay based on carbon isotopic analysis. *Value Eng.* 34, 317–320. doi: 10.14018/j.cnki.cn13-1085/n.2013.19.004

Cavanaugh, K. C., Dangremond, E. M., Doughty, C. L., Williams, A. P., Parker, J. D., Hayes, M. A., et al. (2019). Climate-driven regime shifts in a mangrove-salt marsh ecotone over the past 250 years. *Proc. Natl. Acad. Sci. U. S. A.* 116, 21602–21608. doi: 10.1073/pnas.1902181116

Chen, L., Fan, H., Su, Z., Lin, Q., and Tao, Y. (2021). "Enhancing carbon storage in mangrove ecosystems of China through sustainable restoration and aquaculture actions," in *Wetland Carbon and Environmental Management*. Eds. K. W. Krauss, Z. Zhu and C. L. Stagg (The American Geophysical Union, American), 127–141.

Cloern, J. E., Canuel, E. A., and Harris, D. (2002). Stable carbon and nitrogen isotope composition of aquatic and terrestrial plants of the San Francisco Bay estuarine system. *Limnol. Oceanogr.* 47, 713–729. doi: 10.4319/lo.2002.47.3.0713

Collins, D. S., Avdis, A., Allison, P. A., Johnson, H. D., Hill, J., Piggott, M. D., et al. (2017). Tidal dynamics and mangrove carbon sequestration during the Oligo–Miocene in the South China Sea. *Nat. Commun.* 8, 15698. doi: 10.1038/ncomms15698

Comeaux, R. S., Allison, M. A., and Bianchi, T. S. (2012). Mangrove expansion in the Gulf of Mexico with climate change: Implications for wetland health and resistance to rising sea levels. *Estuarine Coast. Shelf Sci.* 96, 81–95. doi: 10.1016/j.ecss.2011.10.003

Cui, L., Sun, H., Du, X., Feng, W., Wang, Y., Zhang, J., et al. (2021). Dynamics of labile soil organic carbon during the development of mangrove and salt marsh ecosystems. *Ecol. Indic.* 129, 107875. doi: 10.1016/j.ecolind.2021.107875

Dittmar, T., and Lara, R. J. (2001). Molecular evidence for lignin degradation in sulfate-reducing mangrove sediments (Amazonia, Brazil). *Geochim. Cosmochim. Acta* 65, 1417–1428. doi: 10.1016/S0016-7037(00)00619-0

Doughty, C. L., Langley, J. A., Walker, W. S., Feller, I. C., Schaub, R., and Chapman, S. K. (2015). Mangrove range expansion rapidly increases coastal wetland carbon storage. *Estuaries Coasts* 39, 385–396. doi: 10.1007/s12237-015-9993-8

Ellison, J. C. (2008). Long-term retrospection on mangrove development using sediment cores and pollen analysis: A review. *Aquat. Bot.* 89, 93–104. doi: 10.1016/j.aquabot.2008.02.007

Fan, H., He, B., and Pernetta, J. C. (2013). Mangrove ecofarming in Guangxi Province China: an innovative approach to sustainable mangrove use. *Ocean Coast. Manage.* 85, 201–208. doi: 10.1016/j.ocecoaman.2013.04.009

Fan, L. F., Chen, C. P., Yang, M. C., Qiu, G., Liao, Y. Y., and Hsieh, H. L. (2017). Ontogenetic changes in dietary carbon sources and trophic position of two co-occurring horseshoe crab species in southwestern China. *Aquat. Biol.* 26, 15–26. doi: 10.3354/ab00670

Feng, B., Tao, Y., Xie, X., Qin, Y., Hu, B., Jia, R., et al. (2024). Identification of suitable mangrove distribution areas and estimation of carbon stocks for mangrove protection and restoration action plan in China. *J. Mar. Sci. Eng.* 12, 445. doi: 10.3390/jmse12030445

Feng, J., Wang, S., Wang, S., Ying, R., Yin, F., Jiang, L., et al. (2019). Effects of Invasive Spartina alterniflora Loisel. and Subsequent Ecological Replacement by Sonneratia apetala Buch.-Ham. on Soil Organic Carbon Fractions and Stock. *Forests* 10, 171. doi: 10.3390/f10020171

Friesen, S. D., Dunn, C., and Freeman, C. (2018). Decomposition as a regulator of carbon accretion in mangroves: a review. *Ecol. Eng.* 114, 173–178. doi: 10.1016/j.ecoleng.2017.06.069

Gao, Y., Zhou, J., Wang, L., Guo, J., Feng, J., Wu, H., et al. (2019). Distribution patterns and controlling factors for the soil organic carbon in four mangrove forests of China. *Glob. Ecol. Conserv.* 17, 1–14. doi: 10.1016/j.gecco.2019.e00575

Gilman, E., Ellison, J., and Coleman, R. (2007). Assessment of mangrove response to projected relative sea-level rise and recent historical reconstruction of shoreline position. *Environ. Monit. Assess.* 124, 105–130. doi: 10.1007/s10661-006-9212-y

Giri, C. P., and Long, J. (2014). Mangrove reemergence in the northernmost range limit of eastern Florida. *Proc. Natl. Acad. Sci.* 111. doi: 10.1073/pnas.1400687111

Goldberg, L., Lagomasino, D., Thomas, N., and Fatoyinbo, T. (2020). Global declines in human-driven mangrove loss. *Global Change Biol.* 26, 5844–5855. doi: 10.1111/gcb.15275

Hedges, J. I., Blanchette, R. A., Weliky, K., and Devol, A. H. (1988). Effects of fungal degradation on the CuO oxidation products of lignin: a controlled laboratory study. *Geochim. Cosmochim. Acta* 52, 2717–2726. doi: 10.1016/0016-7037(88)90040-3

Hedges, J. I., and Ertel, J. R. (1982). Characterization of lignin by gas capillary chromatography of cupric oxide oxidation products. *Anal. Chem.* 54, 174–178. doi: 10.1021/ac00239a007

Hedges, J. I., and Mann, D. C. (1979). The characterization of plant tissues by their lignin oxidation products. *Geochim. Cosmochim. Acta* 43, 1803–1807. doi: 10.1016/0016-7037(79)90028-0

Hemminga, M. A., and Buth, G. J. C. (1991). Decomposition in salt marsh ecosystems of the SW Netherlands: the effects of biotic and abiotic factors. *Vegetatio* 92, 73–83. doi: 10.1007/BF00047133

Holmer, M., and Olsen, A. B. (2002). Role of decomposition of mangrove and seagrass detritus in sediment carbon and nitrogen cycling in a tropical mangrove forest. *Mar. Ecol.: Prog. Ser.* 230, 87–101. doi: 10.3354/meps230087

Hou, X. Q. (2009). Preliminary study on marine species in liusha bay by using stable carbon and nitrogen isotopes. Guangdong Ocean University, Zhanjiang, 16–17. Ph. D. thesis.

Huang, X. S., Kuang, X. Y., Qin, Z. G., Huang, M. L., and Lin, K. P. (2007). Multi-time-scale variations of recent centenary series of temperature and precipitation in Guangxi of China. *Adv. Clim. Change Res.* 3, 362–367. doi: 10.3969/j.issn.1673-1719.2007.06.010

Jex, C. N., Pate, G. H., Blyth, A. J., Spencer, R. G. M., Hernes, P. J., Khan, S. J., et al. (2014). Lignin biogeochemistry: from modern processes to Quaternary archives. *Quat. Sci. Rev.* 87, 46–59. doi: 10.1016/j.quascirev.2013.12.028

Jiang, R., Wu, Y., and Chen, P. (2021). Study on distribution of sediment carbon and nitrogen in mangrove wetland of Qi'ao Island, Pearl River Estuary. *South China Fish. Sci.* 17, 1–9. doi: 10.12131/20200143

Jones, J. A., Cherry, J. A., and McKee, K. L. (2016). Species and tissue type regulate long-term decomposition of brackish marsh plants grown under elevated CO2 conditions. *Estuar. Coast. Shelf Sci.* 169, 38–45. doi: 10.1016/j.ecss.2015.11.033

Jonge, C. D., Stadnitskaia, A., Hopmans, E. C., Cherkashov, G., Fedotov, A., Streletskaya, I. D., et al. (2015). Drastic changes in the distribution of branched tetraether lipids in suspended matter and sediments from the Yenisei River and Kara Sea (Siberia): Implications for the use of brGDGT-based proxies in coastal marine sediments. *Geochim. Cosmochim. Acta* 165, 200–225. doi: 10.1016/j.gca.2015.05.044

Kauffman, J. B., Adame, M. F., Arifanti, V. B., SChile-Beers, L. M., Bernardino, A. F., Bhomia, R. K., et al. (2020). Total ecosystem carbon stocks of mangroves across broad global environmental and physical gradients. *Ecol. Monogr.* 90, e01405. doi: 10.1002/ecm.1405

Kauffman, J. B., Heider, C., Cole, T. G., Dwire, K. A., and Donato, D. C. (2011). Ecosystem carbon stocks of Micronesian mangrove forests. *Wetlands* 31, 343–352. doi: 10.1007/s13157-011-0148-9

Krauss, K. W., McKee, K. L., Lovelock, C. E., Cahoon, D. R., Saintilan, N., Reef, R., et al. (2014). How mangrove forests adjust to rising sea level. *New Phytol.* 202, 19–34. doi: 10.1111/nph.12605

Kusumaningtyas, M. A., Hutahaean, A. A., Fischer, H. W., Pérez-Mayo, M., Ransby, D., and Jennerjahn, T. C. (2019). Variability in the organic carbon stocks, sources, and accumulation rates of Indonesian mangrove ecosystems. *Estuar. Coast. Shelf Sci.* 218, 310–323. doi: 10.1016/j.ecss.2018.12.007

Lamb, A. L., Wilson, G. P., and Leng, M. J. (2006). A review of coastal palaeoclimate and relative sea-level reconstructions using δ13C and C/N ratios in organic material. *Earth-Sci. Rev.* 75, 29–57. doi: 10.1016/j.earscirev.2005.10.003

Li, Z., Li, Y., Zan, Q., and Yu, S. (2017). A comparison of mangrove community distribution and landscape pattern between Futian and Maipo Nature Reserve at Shenzhen Bay. *Acta Sci. Nat. Univ. Sunyatseni* 56, 12–19. doi: 10.13471/j.cnki.acta.snus.2017.05.002

Li, S., Meng, X., Ge, Z., and Zhang, L. (2015). Vulnerability assessment of the coastal mangrove ecosystems in Guangxi, China, to sea-level rise. *Reg. Envir. Change* 15, 265–275. doi: 10.1007/s10113-014-0639-3

Li, Z., Zhang, Z., Li, J., Zhang, Y., Li, Z., Liu, L., et al. (2008). Pollen distribution in surface sediments of a mangrove system, Yingluo Bay, Guangxi, China. *Rev. Palaeobot. Palynology* 152, 21–31. doi: 10.1016/j.revpalbo.2008.04.001

Liu, H., Ren, H., Hui, D., Wang, W., Liao, B., and Cao, Q. (2014). Carbon stocks and potential carbon storage in the mangrove forests of China. *J. Environ. Manage.* 133, 86–93. doi: 10.1016/j.jenvman.2013.11.037

Lourençato, L. F., Bernardes, M. C., Buch, A. C., and Silva-Filho, E. V. (2019). Lignin phenols in the paleoenvironmental reconstruction of high mountain peatlands from Atlantic Rainforest, SE-Brazil. *Catena* 172, 509–515. doi: 10.1016/j.catena.2018.09.013

Lowman, H., Moingt, M., Lucotte, M., Melack, J., and Page, H. M. (2021). Terrestrial organic matter inputs to nearshore marine sediment under prolonged drought followed by significant rainfall as indicated by lignin. *Estuaries Coasts* 44, 2159–2172. doi: 10.1007/s12237-021-00931-4

Ma, W., Wang, M., Fu, H., Tang, C., and Wang, W. (2022). Predicting changes in molluscan spatial distributions in mangrove forests in response to sea level rise. *Ecol. Evol.* 12. doi: 10.1002/ece3.9033

Marchand, C., Baltzer, F., Lallier-Vergès, E., and Albéric, P. (2004). Pore-water chemistry in mangrove sediments: relationship with species composition and developmental stages (French Guiana). *Mar. Geol.* 208, 361–381. doi: 10.1016/j.margeo.2004.04.015

Marchand, C., Lallier-Vergès, E., Baltzer, F., Albéric, P., Cossa, D., and Baillif, P. (2006). Heavy metals distribution in mangrove sediments along the mobile coastline of French Guiana. *Mar. Chem.* 98, 1–17. doi: 10.1016/j.marchem.2005.06.001

Medina-Contreras, D., Arenas, F., and Sánchez, A. (2024). "Mangrove food webStructure and isotopic niche," in *Treatise on estuarine and coastal science*, *2nd edition*. Eds. D. Baird and M. Elliott (Elsevier, London).

Meng, X., Xia, P., Li, Z., and Meng, D. (2016). Mangrove degradation and response to anthropogenic disturbance in the Maowei Sea (SW China) since 1926 AD: Mangrove-derived OM and pollen. *Org. Geochem.* 98, 166–175. doi: 10.1016/j.orggeochem.2016.06.001

Meyers, P. A. (1994). Preservation of elemental and isotopic source identification of sedimentary organic matter. *Chem. Geol.* 114, 289–302. doi: 10.1016/0009-2541(94)90059-0

Ouyang, X., and Guo, F. (2016). Paradigms of mangroves in treatment of anthropogenic wastewater pollution. *Sci. Total Environ.* 544, 971–979. doi: 10.1016/j.scitotenv.2015.12.013

Palacios Peñaranda, M. L., Cantera Kintz, J. R., and Peña Salamanca, E. J. (2019). Carbon stocks in mangrove forests of the Colombian Pacific. *Estuar. Coast. Shelf Sci.* 227, 106299. doi: 10.1016/j.ecss.2019.106299

Parnell, A. C., and Inger, R. (2016). *Stable Isotope Mixing Models in R with simmr*. Available online at: https://cran.r-project.org/web/packages/simmr/vignettes/simmr.html. (Accessed October 27 2023).

Parnell, A. C., Phillips, D. L., Bearhop, S., Semmens, B. X., Ward, E. J., Moore, J. W., et al. (2013). Bayesian stable isotope mixing models. *Environmetrics* 24, 387–399. doi: 10.1002/env.2221

Peneva-Reed, E. I., Krauss, K. W., Bullock, E. L., Zhu, Z., Woltz, V. L., Drexler, J. Z., et al. (2021). Carbon stock losses and recovery observed for a mangrove ecosystem following a major hurricane in Southwest Florida. *Estuar. Coast. Shelf Sci.* 248, 106750. doi: 10.1016/j.ecss.2020.106750

Perera, K. A. R. S., and Amarasinghe, M. D. (2019). Carbon sequestration capacity of mangrove soils in micro tidal estuaries and lagoons: A case study from Sri Lanka. *Geoderma* 347, 80–89. doi: 10.1016/j.geoderma.2019.03.041

Perera, K. A. R. S., De Silva, K. H. W. L., and Amarasinghe, M. D. (2018). Potential impact of predicted sea level rise on carbon sink function of mangrove ecosystems with special reference to Negombo estuary, Sri Lanka. *Global Planet. Change* 161, 162–171. doi: 10.1016/j.gloplacha.2017.12.016

Perez, A., Libardoni, B. G., and Sanders, C. J. (2018). Factors influencing organic carbon accumulation in mangrove ecosystems. *Biol. Lett.* 14. doi: 10.1098/rsbl.2018.0237

Prasad, M. B. K., and Ramanathan, A. L. (2009). Organic matter characterization in a tropical estuarine-mangrove ecosystem of India: Preliminary assessment by using stable isotopes and lignin phenols. Estuarine. *Coast. Shelf Sci.* 84, 617–624. doi: 10.1016/j.ecss.2009.07.029

Rovai, A. S., Coelho-Jr, C., de Almeida, R., Cunha-Lignon, M., Menghini, R. P., Twilley, R. R., et al. (2021). Ecosystem-level carbon stocks and sequestration rates in mangroves in the Cananéia-Iguape lagoon estuarine system, southeastern Brazil. *For. Ecol. Manage.* 479, 118553. doi: 10.1016/j.foreco.2020.118553

Sánchez, A., and Gómez-León, A. (2024). Azoic sediments and benthic foraminifera: Environmental quality in a subtropical coastal lagoon in the gulf of California. *Environ. Res.* 244. doi: 10.1016/j.envres.2023.117924

Sánchez, A., Gonzalez-Jones, P., Camacho-Cruz, K. A., Anguas-Cabrera, D., Ortiz-Hernández, M. C., and Rey-Villiers, N. (2023). Influence of pelagic sargassum influxes on the δ15N in Thalassia testudinum of the Mexican Caribbean coastal ecosystem. *Mar. pollut. Bull.* 192, 115091. doi: 10.1016/j.marpolbul.2023.115091

Sanders, C. J., Smoak, J. M., Waters, M. N., Sanders, L. M., Brandini, N., and Patchineelam, S. R. (2012). Organic matter content and particle size modifications in mangrove sediments as responses to sea level rise. *Mar. Environ. Res.* 77, 150–155. doi: 10.1016/j.marenvres.2012.02.004

Santos-Andrade, M., Hatje, V., Arias-Ortiz, A., Patire, V. F., and da Silva, L. A. (2021). Human disturbance drives loss of soil organic matter and changes its stability and sources in mangroves. *Environ. Res.* 202, 111663. doi: 10.1016/j.envres.2021.111663

Sasmito, S. D., Kuzyakov, Y., Lubis, A. A., Murdiyarso, D., Hutley, L. B., Bachri, S., et al. (2020). Organic carbon burial and sources in soils of coastal mudflat and mangrove ecosystems. *Catena* 187, 104414. doi: 10.1016/j.catena.2019.104414

Senger, D. F., Saavedra Hortua, D. A., Engel, S., Schnurawa, M., Moosdorf, N., and Gillis, L. G. (2021). Impacts of wetland dieback on carbon dynamics: A comparison between intact and degraded mangroves. *Sci. Total Environ.* 753, 141817. doi: 10.1016/j.scitotenv.2020.141817

Shepard, F. P. (1954). Nomenclature based on sand-silt-clay ratios. *J. Sediment. Res.* 24, 151–158. doi: 10.1306/D4269774-2B26-11D7-8648000102C1865D

Stringer, C. E., Trettin, C. C., and Zarnoch, S. J. (2016). Soil properties of mangroves in contrasting geomorphic settings within the Zambezi River Delta, Mozambique. *Wetlands Ecol. Manage.* 24, 139–152. doi: 10.1007/s11273-015-9478-3

Su, Z., Qiu, G., Fan, H., Li, M., and Fang, C. (2020). Changes in carbon storage and macrobenthic communities in a mangrove-seagrass ecosystem after the invasion of

smooth cordgrass in southern China. *Mar. pollut. Bull.* 152. doi: 10.1016/j.marpolbul.2020.110887

Suello, R. H., Hernandez, S. L., Bouillon, S., Belliard, J.-P., Dominguez-Granda, L., Van de Broek, M., et al. (2022). Mangrove sediment organic carbon storage and sources in relation to forest age and position along a deltaic salinity gradient. *Biogeosciences* 19, 1571–1585. doi: 10.5194/bg-19-1571-2022

Sun, H., Jiang, J., Cui, L., Feng, W., Wang, Y., and Zhang, J. (2019). Soil organic carbon stabilization mechanisms in a subtropical mangrove and salt marsh ecosystems. *Sci. Total Environ.* 673, 502–510. doi: 10.1016/j.scitotenv.2019.04.122

Tareq, S. M., Tanaka, N., and Ohta, K. (2004). Biomarker signature in tropical wetland: lignin phenol vegetation index (LPVI) and its implications for reconstructing the paleoenvironment. *Sci. Total Environ.* 324, 91–103. doi: 10.1016/j.scitotenv.2003.10.020

Tian, Y., Huang, H., Zhou, G., Zhang, Q., Tao, J., Zhang, Y., et al. (2021). Aboveground mangrove biomass estimation in Beibu Gulf using machine learning and UAV remote sensing. *Sci. Total Environ.* 781. doi: 10.1016/j.scitotenv.2021.146816

Valéry, L., Bouchard, V., and Lefeuvre, J. C. (2004). Impact of the invasive native species Elymus athericus on carbon pools in a salt marsh. *Wetlands* 24, 268–276. doi: 10.1672/0277-5212(2004)024[0268:IOTINS]2.0.CO;2

Vaughn, D. R., Bianchi, T. S., Shields, M. R., Kenney, W. F., and Osborne, T. Z. (2020). Increased organic carbon burial in northern Florida mangrove-salt marsh transition zones. *Glob. Biogeochem. Cycles.* 34, e2019GB006334. doi: 10.1029/2019gb006334

Versteegh, G. J. M., Schefuß, E., Dupont, L., Marret, F., Sinninghe Damsté, J. S., and Jansen, J. H. F. (2004). Taraxerol and Rhizophora pollen as proxies for tracking past mangrove ecosystems. *Geochim. Cosmochim. Acta* 68, 411–422. doi: 10.1016/s0016-7037(03)00456-3

Wang, Y.-S., and Gu, J.-D. (2021). Ecological responses, adaptation and mechanisms of mangrove wetland ecosystem to global climate change and anthropogenic activities. *Int. Biodeterior. Biodegrad.* 162, 105248. doi: 10.1016/j.ibiod.2021.105248

Wang, G., Guan, D., Peart, M. R., Chen, Y., and Peng, Y. (2013). Ecosystem carbon stocks of mangrove forest in Yingluo Bay, Guangdong Province of South China. *For. Ecol. Manage.* 310, 539–546. doi: 10.1016/j.foreco.2013.08.045

Wang, G., Guan, D., Xiao, L., and Peart, M. R. (2019). Ecosystem carbon storage affected by intertidal locations and climatic factors in three estuarine mangrove forests of South China. *Reg. Envir. Change* 19, 1701–1712. doi: 10.1007/s10113-019-01515-6

Wang, G., Singh, M., Wang, J., Xiao, L., and Guan, D. (2021). Effects of marine pollution, climate, and tidal range on biomass and sediment organic carbon in Chinese mangrove forests. *Catena* 202, 105270. doi: 10.1016/j.catena.2021.105270

Ward, R. D., Friess, D. A., Day, R. H., and Mackenzie, R. A. (2016). Impacts of climate change on mangrove ecosystems: a region by region overview. *Ecosyst. Health Sustain.* 2. doi: 10.1002/ehs2.1211

Xia, P., Meng, X., Li, Z., Feng, A., Yin, P., and Zhang, Y. (2015). Mangrove development and its response to environmental change in Yingluo Bay (SW China) during the last 150years: Stable carbon isotopes and mangrove pollen. *Org. Geochem.* 85, 32–41. doi: 10.1016/j.orggeochem.2015.04.003

Xia, P., Meng, X., Li, Z., Zhi, P., Zhao, M., and Wang, E. (2019). Late Holocene mangrove development and response to sea level change in the northwestern South China Sea. *Acta Oceanol. Sin.* 38, 111–120. doi: 10.1007/s13131-019-1359-9

Xia, S., Song, Z., Wang, W., Fan, Y., Guo, L., Van Zwieten, L., et al. (2023). Patterns and determinants of plant-derived lignin phenols in coastal wetlands: Implications for organic C accumulation. *Funct. Ecol.* 37, 1067–1081. doi: 10.1111/1365-2435.14290

Xin, K., Yan, K., Gao, C., and Li, Z. (2018). Carbon storage and its influencing factors in Hainan Dongzhangang mangrove wetlands. *Mar. Freshw. Res.* 69, 771–779. doi: 10.1071/mf17101

Xiong, Y., Liao, B., Proffitt, E., Guan, W., Sun, Y., Wang, F., et al. (2018a). Soil carbon storage in mangroves is primarily controlled by soil properties: A study at Dongzhai Bay, China. *Sci. Total Environ.* 619-620, 1226–1235. doi: 10.1016/j.scitotenv.2017.11.187

Xiong, Y., Liao, B., and Wang, F. (2018b). Mangrove vegetation enhances soil carbon storage primarily through *in situ* inputs rather than increasing allochthonous sediments. *Mar. pollut. Bull.* 131, 378–385. doi: 10.1016/j.marpolbul.2018.04.043

Xu, L., Wang, M., Xin, C., Liu, C., and Wang, W. (2020). Mangrove distribution in relation to seasonal water salinity and ion compartmentation: a field study along a freshwater-dominated river. *Hydrobiologia* 847, 549–561. doi: 10.1007/s10750-019-04119-7

Yan, L., Xie, X., Heiss, J. W., Peng, K., Deng, Y., Gan, Y., et al. (2023). Isotopic and spectral signatures unravel the sources, preservation and degradation of sedimentary organic matter in the Dongzhai Harbor mangrove estuary, southern China. *J. Hydrol.* 618. doi: 10.1016/j.jhydrol.2023.129256

Yan, R., Feng, J., Fu, T., Chen, Q., Wang, Z., Kang, F., et al. (2024). Spatial variation of organic carbon storage and aggregate sizes in the sediment of the Zhangjiang mangrove ecosystem. *Catena* 234, 107545. doi: 10.1016/j.catena.2023.107545

Zhao, X., Chen, Z., Xu, Y., Zhai, X., Song, X., Xu, H., et al. (2023). Linkages between organic carbon composition and microbial community structure in two contrasting subtropical mangrove sediments in southern China. *Reg. Stud. Mar. Sci.* 66, 103159. doi: 10.1016/j.rsma.2023.103159

Zheng, Y., and Takeuchi, W. (2020). Quantitative assessment and driving force analysis of mangrove forest changes in China from 1985 to 2018 by integrating optical and radar imagery. *ISPRS Int. J. Geo-Inf.* 9, 1–17. doi: 10.3390/ijgi9090513

Zhu, Y., Zhao, F., Guo, J., Wu, G., and Lin, G. (2016). Below-groundorganic carbon distribution and burial characteristics of the Gaoqiao mangrove area in Zhanjiang, Guangdong, southern China. *Acta Ecol. Sin.* 36, 7841–7849. doi: 10.5846/stxb201511102276